Activation of ADF/cofilin by phosphorylation-regulated Slingshot phosphatase is required for the meiotic spindle assembly in *Xenopus laevis* oocytes

Shohei Iwase[a], Ryuhei Sato[a], Pieter-Jan De Bock[b,c], Kris Gevaert[b,c], Saburo Fujiki[a], Toshinobu Tawada[a], Miyako Kuchitsu[d], Yuka Yamagishi[d], Shoichiro Ono[e], and Hiroshi Abe[a,d]

[a]Department of Nanobiology, Graduate School of Advanced Integration Science, and [d]Department of Biology, Faculty of Science, Chiba University, Chiba 263-8522, Japan; [b]VIB Department of Medical Protein Research and [c]Department of Biochemistry, Ghent University, B-9000 Ghent, Belgium; [e]Department of Pathology, Emory University, Atlanta, GA 30322

ABSTRACT **We identify *Xenopus* ADF/cofilin (XAC) and its activator, Slingshot phosphatase (XSSH), as key regulators of actin dynamics essential for spindle microtubule assembly during *Xenopus* oocyte maturation. Phosphorylation of XSSH at multiple sites within the tail domain occurs just after germinal vesicle breakdown (GVBD) and is accompanied by dephosphorylation of XAC, which was mostly phosphorylated in immature oocytes. This XAC dephosphorylation after GVBD is completely suppressed by latrunculin B, an actin monomer–sequestering drug. On the other hand, jasplakinolide, an F-actin–stabilizing drug, induces dephosphorylation of XAC. Effects of latrunculin B and jasplakinolide are reconstituted in cytostatic factor–arrested extracts (CSF extracts), and XAC dephosphorylation is abolished by depletion of XSSH from CSF extracts, suggesting that XSSH functions as an actin filament sensor to facilitate actin filament dynamics via XAC activation. Injection of anti-XSSH antibody, which blocks full phosphorylation of XSSH after GVBD, inhibits both meiotic spindle formation and XAC dephosphorylation. Coinjection of constitutively active XAC with the antibody suppresses this phenotype. Treatment of oocytes with jasplakinolide also impairs spindle formation. These results strongly suggest that elevation of actin dynamics by XAC activation through XSSH phosphorylation is required for meiotic spindle assembly in *Xenopus laevis*.**

Monitoring Editor
Fred Chang
Columbia University

Received: Dec 5, 2012
Revised: Mar 26, 2013
Accepted: Apr 17, 2013

INTRODUCTION

Oocyte maturation is defined by reinitiation of meiosis to release oocytes from arrest in meiotic prophase I (Pro I). This process starts with the breakdown of the nuclear envelope of the germinal vesicle, a giant nucleus specifically formed in oocytes (i.e., germinal vesicle breakdown [GVBD] or nuclear envelope breakdown). In many vertebrates, external hormonal stimuli activate intracellular signaling pathways responsible for the activation of maturation-promoting factor (MPF), which is composed of cyclin B and $p34^{cdc2}$ (Cdk1) and promotes GVBD (Masui and Markert, 1971; Lohka *et al.*, 1988; Dorée and Hunt, 2002). Entrance of MPF into nuclei to phosphorylate nuclear lamins and nuclear pore complex proteins is essential for GVBD (Margalit *et al.*, 2005). In *Xenopus* oocytes, progesterone-induced activation of MPF triggers GVBD, chromosome condensation, spindle formation, and progression to metaphase II (Masui and Clark, 1979), and the white maturation spot formation at the animal pole is a well-established indicator of GVBD. The nucleoplasm released to the cytoplasm after GVBD forms the yolk-free zone at the animal region, and chromosomes are transported to the animal cortex to form meiotic spindles. Microtubules play essential roles in this process. A disk-shaped organelle called the microtubule-organizing center and transient microtubule array (MTOC-TMA) assembles in

This article was published online ahead of print in MBoC in Press (http://www.molbiolcell.org/cgi/doi/10.1091/mbc.E12-12-0851) on April 24, 2013.

Address correspondence to: Hiroshi Abe (habe@faculty.chiba-u.jp).

Abbreviations used: ADF, actin-depolymerizing factor; CSF, cytostatic factor; GST, glutathione *S*-transferase; GVBD, germinal vesicle breakdown; jas, jasplakinolide; lat B, latrunculin B; Meta II, metaphase II; MS, mass spectrometry; MTOC-TMA, microtubule-organizing center and transient microtubule array; pha, phalloidin; XAC, *Xenopus* ADF/cofilin; XSSH, *Xenopus* Slingshot.

the yolk-free zone to capture chromosomes in the cytoplasm (Jessus *et al.*, 1986; Gard, 1992; Gard *et al.*, 1995). Then MTOC-TMA disappears, and chromosomes are aligned on the spindle microtubules.

Actin filaments play crucial roles during oocyte maturation (for review see Sun and Schatten, 2006). In *Xenopus* oocytes, although the regulation of actin dynamics remains to be clarified, actin filaments are reportedly required for spindle migration and rotation (Ryabova *et al.*, 1986; Gard *et al.*, 1995). The significance of actin filaments in these processes is well studied in mouse oocytes. The meiotic spindle forms in the center of oocytes after GVBD and then begins to migrate toward the cortex (Verlhac *et al.*, 2000). This migration is specifically inhibited by the addition of cytochalasin B or D, which induces disassembly of actin filaments, although GVBD occurs, and the meiotic spindle forms in the center of oocytes (Longo and Chen, 1985; Verlhac *et al.*, 2000; Liu *et al.*, 2002; Calarco, 2005). Because colchicine or nocodazole treatment disrupts spindle microtubules but not chromosome condensation and migration of chromosomes to the cortex, polarized movement of chromosomes wholly depends on a process mediated by actin filaments (Longo and Chen, 1985; Verlhac *et al.*, 2000). The cortical actin filaments are essential for peripheral spindle anchorage in murine oocytes. Meiotic chromosomes migrating to the cortex signals the cortical domain near the chromosomes to form a thick cortical actin filament layer called the actin cap (Longo and Chen, 1985; Deng *et al.*, 2007; Deng and Li, 2009). Recently the actin cap-inducing signal from chromosomes was postulated to be the activation of the Arp2/3 complex, an actin nucleator, in a Ran-GTPase–dependent manner (Yi *et al.*, 2011). This complex localizes to the cortical actin cap, where it nucleates actin filaments. Inhibition of Arp2/3 activity leads to rapid dissociation of the spindle from the cortex, indicating that maintenance of subcortical localization of meiotic spindles also depends on Arp2/3 complex activity.

The function of actin filaments deeper in the cytoplasm of oocytes is beginning to be understood (for review see Field and Lénárt, 2011). During the progression of oocyte maturation, formation of cytoplasmic actin filaments mediated by Formin-2 and Spire is necessary for spindle migration to the cortex in mouse oocytes (Azoury *et al.*, 2008, 2011; Schuh and Ellenberg, 2008; Pfender *et al.*, 2011) and in *Drosophila* oocytes (Dahlgaard *et al.*, 2007). In mouse oocytes, the cytoplasmic actin meshwork, which is dense in prophase I, dramatically decreases by meiosis resumption and then re-forms in late meiosis I (Azoury *et al.*, 2011). This meshwork remodeling correlates with Formin-2 degradation and reaccumulation. Overexpression of Formin-2 during oocyte maturation maintains the meshwork density and prevents spindle migration. On the other hand, depletion of Spire proteins, which cooperate with Formin-2, also prevents spindle migration (Pfender *et al.*, 2011). Suppression of spindle migration by either up-regulation or down-regulation of actin nucleators indicates that actin filament dynamics is an important factor for directional spindle transport.

In addition to the role of actin filaments in spindle migration, a three-dimensional actin meshwork formed after GVBD in the nuclear region is required for chromosome congression in starfish oocytes (Lénárt *et al.*, 2005). Contraction of this meshwork delivers chromosomes to the spindle microtubule array. Whereas this meshwork contracts homogeneously and isotropically throughout the nuclear space, mechanical anchorage of this meshwork to the closest cell cortex translates the homogeneous contraction into asymmetrical, directional transport of chromosomes (Mori *et al.*, 2011). Important roles of actin filaments on chromosome congression and spindle migration are also reported in ascidian oocytes (Prodon *et al.*, 2008, 2009). In these species, actin filaments, which are absent in Pro I nuclei, rapidly assemble just after GVBD in the nuclear region. In *Xenopus* oocytes, however, a dense actin filament meshwork is present in nuclei of Pro I oocytes (Bohnsack *et al.*, 2006; Miyamoto *et al.*, 2011). This intranuclear accumulation of actin filaments is due to lack of exportin 6, which is responsible for exclusion of actin from nuclei in somatic cells, since injection of exportin 6 into nuclei has been shown to cause actin filaments to disappear, thereby increasing the fragility of nuclei. Thus the actin network that spans the entire nucleus might mechanically support the extremely large oocyte nucleus in *Xenopus* (Bohnsack *et al.*, 2006). However, the regulation of intranuclear and cytoplasmic actin dynamics remained to be clarified in *Xenopus* oocytes.

We demonstrated that microinjection of phalloidin, an F-actin–stabilizing drug, prevents GVBD in *Xenopus* oocytes treated with progesterone (Okada *et al.*, 2012). Microtubules formed unusual structures in both nuclei and cytoplasm of phalloidin-injected oocytes during oocyte maturation. Therefore intranuclear and cytoplasmic actin filament dynamics appear to be required for the completion of GVBD and critically involved in the regulation of microtubule assembly during *Xenopus* oocyte maturation. Many actin-binding proteins are involved in the regulation of intracellular dynamics of actin filaments. The ADF/cofilin family of proteins is an essential factor that severs and depolymerizes actin filaments to increase the rate of actin filament turnover (for reviews see Ono, 2007; Van Troys *et al.*, 2008; Bernstein and Bamburg, 2010). LIM-kinases phosphorylate and inactivate ADF/cofilin (Arber *et al.*, 1998; Yang *et al.*, 1998), whereas Slingshot phosphatases dephosphorylate and reactivate it (Niwa *et al.*, 2002). In *Xenopus* oocytes, the formation of white maturation spots and MTOC-TMA is disrupted by injection of constitutively active LIM-kinases, whereas this phenotype is suppressed by coinjection of a constitutively active form of ADF/cofilin (Takahashi *et al.*, 2001). This suggests that the dynamic regulation of actin filaments by ADF/cofilin is involved in progression of oocyte maturation, although the exact role of ADF/cofilin and the molecular mechanism that regulates its activity during oocyte maturation remain to be clarified. Slingshot (SSH) was originally identified as an ADF/cofilin-specific phosphatase in *Drosophila* and humans (Niwa *et al.*, 2002). This protein colocalizes with actin filaments in cultured cells, and its association with actin filaments markedly enhances phosphatase activity (Nagata-Ohashi *et al.*, 2004). Phosphorylation of the SSH C-terminal domain (tail domain) prevents its binding to actin filaments by association of 14-3-3 proteins with the phosphorylation site (Nagata-Ohashi *et al.*, 2004; Soosairajah *et al.*, 2005). *Xenopus* Slingshot (XSSH) is also phosphorylated and activated by binding to actin filaments (Tanaka *et al.*, 2005a,b). In the present study, we examine the role of XSSH phosphorylation and find that dephosphorylation of *Xenopus* ADF/cofilin (XAC) through XSSH regulated by phosphorylation induces actin dynamics essential for spindle microtubule assembly during oocyte maturation in *Xenopus laevis*.

RESULTS

Phosphorylation states of XAC and XSSH during oocyte maturation

We first analyzed the phosphorylation states of XAC and its activator, XSSH, during oocyte maturation, since ADF/cofilin is a key regulator for actin dynamics and is mostly phosphorylated (inactivated) in oocytes (Abe *et al.*, 1996). As shown in Figure 1A, stage VI oocytes contain three-fourths of XAC in the phosphorylated form (Figure 1A, a), but more XAC is dephosphorylated than phosphorylated in unfertilized eggs (matured oocytes; Figure 1A, b). During

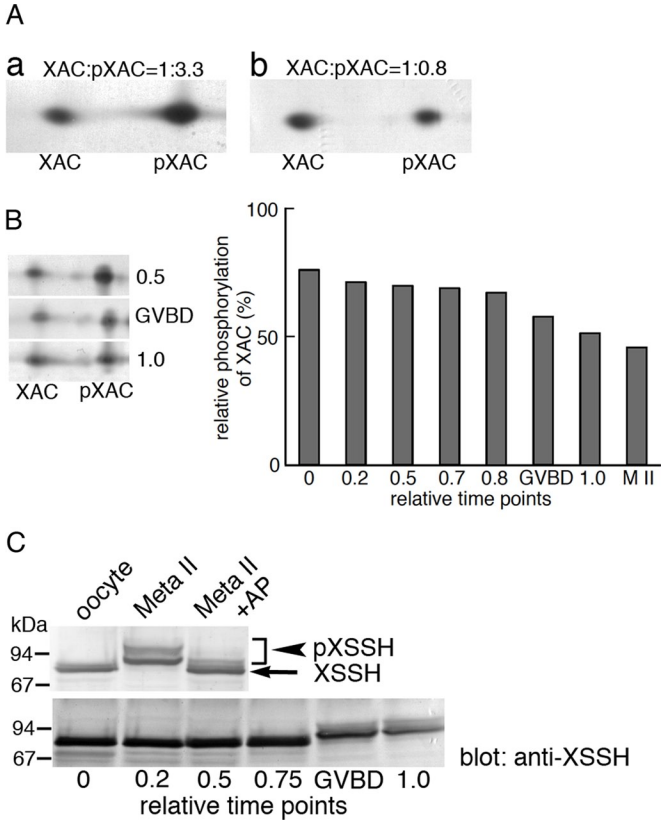

FIGURE 1: Phosphorylation states of XAC and XSSH during oocyte maturation. (A) Phosphorylation states of XAC as determined by 2D immunoblots in immature oocytes (a) and mature (Meta II) oocytes (b). Unphosphorylated and phosphorylated forms of XAC are indicated by XAC and pXAC, respectively. Relative amounts of XAC and pXAC were determined by densitometry and are indicated on top of each blot. (B) Time course of changes in phosphorylation levels of XAC during oocyte maturation. Left, three examples of 2D immunoblots of XAC at relative time points as indicated in the graph on the right. The spots of XAC and pXAC at different time points during oocyte maturation were quantified by densitometry, and percentages of pXAC are shown. Time 0 is at the addition of progesterone, and time 1.0 is when >80% of oocytes show WMS. GVBD represents the oocytes in which GVBD just occurred. M II represents the data from fully mature oocytes. (C) Phosphorylation states of XSSH during oocyte maturation as determined by mobility shifts in immunoblot. Top, immunoblots of XSSH in immature (oocyte) and mature (Meta II) oocytes. XSSH in mature oocyte were detected as bands with slower mobility than those of XSSH in immature oocytes. The retarded mobility was canceled by alkaline phosphatase treatment (Meta II + AP), indicating that the mobility shifts were due to phosphorylation. The bands of pXSSH were split into two groups. Bottom, immunoblots of XSSH at different time points during oocyte maturation. Phosphorylation of XSSH as shown by mobility shifts was enhanced at GVBD.

oocyte maturation, high levels of XAC phosphorylation are maintained in immature oocytes until GVBD, whereas this balance is shifted toward dephosphorylation after GVBD, and finally XAC phosphorylation reaches its lowest level in unfertilized eggs (M II; Figure 1B). On the other hand, a drastic difference in the mobility of XSSH on SDS–PAGE is observed between oocytes and unfertilized eggs (Figure 1C, top), and this mobility shift occurs at or after GVBD during oocyte maturation (Figure 1C, bottom). We previously indicated that these mobility shifts are caused by phosphorylation of XSSH (Tanaka *et al.*, 2005a) and again show that the shifted bands with lower mobility disappear on treating egg extracts with alkaline phosphatase (Figure 1C, top). Nearly all XSSH is detected as multiple lower-mobility bands in unfertilized eggs (Figure 1C, top). In addition, these bands are roughly divided into two groups—lower- and higher-mobility groups. As will be shown later (Figure 2), these differences in mobility are derived from the extent of phosphorylation. These results suggest functional correlation between XSSH phosphorylation and XAC dephosphorylation.

The tail domain of XSSH is hyperphosphorylated in mature oocytes

To map maturation-dependent phosphorylation sites in XSSH, we constructed glutathione *S*-transferase (GST)–fused truncated forms of XSSH containing SSH-A and SSH-B domains (GST-AB), lacking the C-terminal tail domain (GST-Δtail), and containing the tail domain alone (GST-tail; Figure 2A). These mutants were tested for phosphorylation using cytostatic factor–arrested extracts (CSF extracts). Because CSF extracts remain arrested at metaphase of meiosis II when XSSH is fully phosphorylated, the unknown "XSSH kinases" are expected to be active. As shown in Figure 2B, a–c, the full-length XSSH (GST-XSSH) is effectively shifted to a low-mobility band in CSF extracts (Figure 2B, b, arrowhead), whereas the shift is abolished by alkaline phosphatase treatment (Figure 2B, c), indicating that maturation-dependent phosphorylation of XSSH could be reproduced in vitro by CSF extracts. Among the tested truncated mutants, only GST-tail exhibits a drastic change in its mobility on SDS–PAGE (Figure 2B, a‴–c‴), although GST-AB (Figure 2B, a′–c′) and GST-Δtail (Figure 2B, a″–c″) also show slight mobility shifts. These bands with lower-mobility shifts disappear when the samples are treated with alkaline phosphatase. Therefore we conclude that the tail domain contains phosphorylation site(s) that cause major phosphorylation-dependent mobility shifts of XSSH during oocyte maturation.

The tail domain was further divided into two regions, designated as GST–N-tail and GST–C-tail (Figure 2A), and each was assayed for mobility shift with CSF extracts. Although both regions were phosphorylated to represent striking mobility shifts (Figure 2C), GST-N-tail is more sensitive to phosphorylation using serially diluted CSF extracts (data not shown). This mobility shift of GST–N-tail is mostly suppressed in interphase extracts but recovered on addition of ΔN85-cyclin B to the interphase extracts, indicating that phosphorylation of GST-N-tail occurs specifically at both meiotic and mitotic phases (Figure 2D). Furthermore, when 1 μM okadaic acid was added to CSF extracts, an additional GST–N-tail band with greater mobility shift was detected (Figure 2D). This suggests that phosphorylation of XSSH is dynamically regulated in CSF extracts. The large mobility shift of GST–N-tail and its degradation products, in addition to the presence of many Ser and Thr residues in its primary sequence (Figure 2E), suggested the presence of multiple phosphorylation sites in this region. Therefore we selected this region for identifying phosphorylation sites using mass spectrometry (MS) analysis. GST–N-tail was treated with CSF extracts and digested by trypsin, and then enriched phosphopeptides were analyzed by liquid chromatography–tandem MS (LC-MS/MS; Supplemental Tables S1 and S2). As shown in Figure 2E, 14 residues (13 Ser or Thr residues and one Tyr residue) were determined as phosphorylation sites. Site-directed mutagenesis studies were consistent with these results (Figure 2, E and F). Independently of the MS analysis, we predicted phosphorylation sites (P1–P5) based on consensus sequences for recognition by $p34^{cdc2}$ kinase, protein kinase D1 (PKD1), and so on, and substituted them with alanine one by one or by clusters. Putative sites P1–P4 were actually phosphorylated, but P5

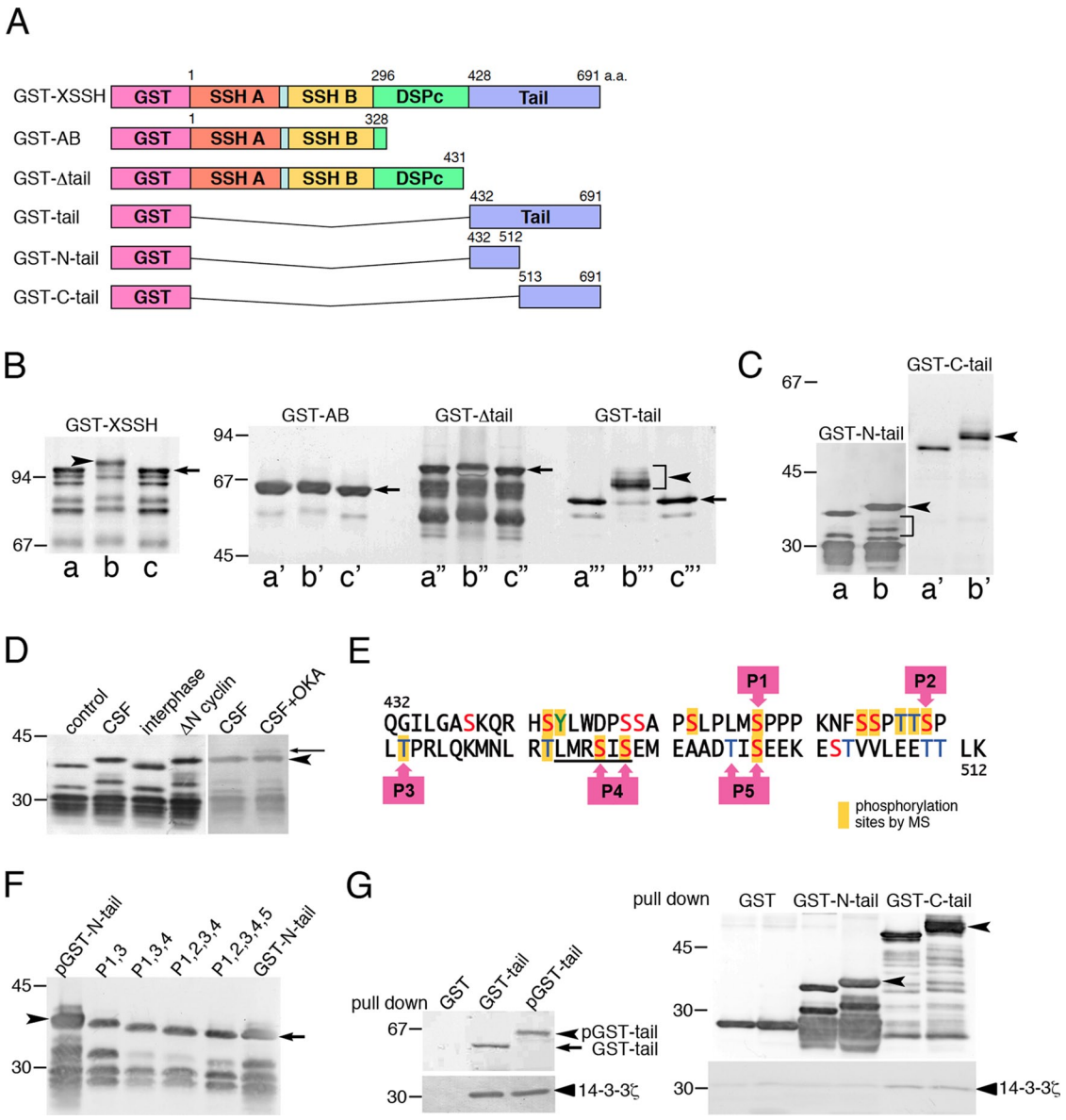

FIGURE 2: Identification of phosphorylation sites of XSSH and binding properties of XSSH to 14-3-3ζ. (A) Domain organization of XSSH and structures of truncated mutants used in this study. SSH a and SSH b, Slingshot-homology domains A and B, respectively; DSPc, a dual-specific phosphatase domain; Tail, Slingshot tail domain. (B, C) Phosphorylation of XSSH and the mutants with CSF extracts. (a–a‴) treatments with buffer alone, (b–b‴) treatments with CSF extracts, and (c–c‴) treatments with CSF extracts followed by alkaline phosphatase treatments. Arrowheads represent shifted bands due to phosphorylation, and arrows indicate the dephosphorylated forms after alkaline phosphatase treatments. Because samples were probed with the anti-GST antibody, degradation products were also detected. Phosphorylation of the degraded GST–N-tail was also detected, as shown by a bracket in C. (D) In vitro phosphorylation of GST–N-tail was performed in buffer alone (control), meiotic extracts (CSF), interphase extracts (interphase), or mitotic extracts (ΔN cyclin) and subjected to immunoblot with anti-GST antibody. In the two right lanes, GST–N-tail was reacted with CSF extracts (CSF) or CSF extracts with 1 μM okadaic acid (CSF+OKA). Arrowhead indicates the position of phosphorylated bands, and an arrow indicates the position of additionally shifted bands in the presence of okadaic acid. (E) Phosphorylation sites in the N-tail region. The yellow boxes indicate phosphorylated residues identified by MS. P1–P5 represent residues examined by site-directed mutagenesis. The underlining at the P4 site indicates the consensus sequence for PKD1 phosphorylation sites. (F) GST–N-tail (pGST–N-tail) and its variants with indicated mutations (P1,3 to P1,2,3,4,5) were phosphorylated in vitro in CSF extracts and subjected to immunoblot with anti-GST antibody. Unphosphorylated GST–N-tail was loaded on the right lane. Arrow and arrowhead indicate nonphosphorylated and fully phosphorylated GST–N-tail, respectively. (G) Pull-down assay of 14-3-3ζ with GST-tail mutants. 14-3-3ζ bound to GST-tail (left) and GST-C-tail (right) before and after phosphorylation but did not bind to GST-N-tail (right). Top right, immunoblots with anti-GST antibody of nonphosphorylated and phosphorylated GST-tail mutants bound to glutathione beads. GST alone was used as control. Arrowheads indicate phosphorylated GST–N-tail and GST-C-tail. Bottom right, coprecipitated 14-3-3ζ probed with anti–14-3-3 antibody.

contained one actual phosphorylation site (Ser-497) and one that was not phosphorylated (Thr-495; Figure 2E). When GST–N-tail variants with these mutations were incubated with CSF extracts, mobility shifts decreased stepwise as more mutations were combined (from double to quintuple mutations). A single mutation at each site caused only a minor decrease in the mobility shift by phosphorylation with CSF extracts (Supplemental Figure S1). Thus differences in mobility shift correlated with distinct levels of XSSH phosphorylation.

In mammalian cells, the SSH1L tail domain is phosphorylated by PKD1 to lead to association with 14-3-3ζ (Eiseler *et al.*, 2009). In the N-tail region of XSSH, PKD1 phosphorylation consensus sequence is also present, and it is indeed phosphorylated (Figure 2E, the P4 site). Therefore we examined the binding of *Xenopus* 14-3-3ζ to the XSSH tail domain. As shown in Figure 2G, unexpectedly, 14-3-3ζ binds to GST-tail without any dependence on its phosphorylation. 14-3-3ζ does not bind to GST–N-tail before and after phosphorylation, whereas association of 14-3-3ζ with the C-tail region is detected independent of its phosphorylation. These results are quite different from the mammalian case.

Phosphorylation of XSSH enhances its affinity for F-actin to elevate phosphatase activity

All studies concerning the Slingshot phosphatase in mammalian cells have reported that its phosphorylation leads to suppression of dephosphorylation of ADF/cofilin. In contrast to these reports, in *Xenopus* oocytes, phosphorylation of XSSH correlated with enhanced dephosphorylation of XAC. We asked whether phosphorylation of XSSH affects its phosphatase activity. The phosphorylated XSSH (pXSSH) used here was prepared by phosphorylation of GST-XSSH in CSF-arrested extracts. As shown in Figure 3A, time course of dephosphorylation of phosphorylated XAC (pXAC) indicates that pXSSH has slightly enhanced phosphatase activity and that both forms of XSSH require the presence of actin filaments for their phosphatase activity (Figure 3A, top three). Therefore we next examined whether phosphorylation of XSSH alters its affinity with actin filaments by F-actin cosedimentation assay. As shown in Figure 3B, cosedimentation of pXSSH with actin filaments is enhanced as compared with that of XSSH, indicating that phosphorylation of XSSH increases its affinity with actin filaments. These results suggest that enhanced association of pXSSH with actin filaments leads to enhancement in XSSH phosphatase activity. On the other hand, when XAC or chick cofilin is added to the mixture of XSSH and actin filaments, cosedimented XSSH in either form is reduced (Figure 3C). Thus XAC competes to some extent with XSSH for binding to actin filaments. Furthermore, addition of chicken cofilin to the assay mixture with actin filaments in a 1:1 M ratio significantly inhibits dephosphorylation of pXAC (Figure 3A, bottom two), suggesting that XSSH phosphatase activity is suppressed by elevating the concentration of dephosphorylated XAC even in the presence of a sufficient amount of pXAC.

XSSH functions as an F-actin sensor to dephosphorylate XAC

To clarify the causal relationship among actin filaments, XSSH, and XAC dephosphorylation, we first examined whether phosphorylation states of XAC are affected, by altering the amount of actin filaments in oocytes with latrunculin B (an actin monomer–sequestering drug inducing actin filament depolymerization) or jasplakinolide (an actin filament–stabilizing drug inducing actin polymerization). As shown in Figure 4A, treatment of immature oocytes, in which XAC is mostly phosphorylated, with jasplakinolide for 1 h induces drastic dephosphorylation of XAC, indicating that increase in the formation of actin filaments alone can induce XAC dephosphorylation. The XAC dephosphorylation after GVBD is strongly suppressed by incubating oocytes with latrunculin B (Figure 4A), which causes depolymerization of actin filaments as judged by the presence of most actin in the high-speed supernatant (Figure 4D). This indicates that XAC dephosphorylation requires actin filaments. These effects by actin drug treatments are reproducible in CSF extracts (Figure 4B). The amount of phosphorylated XAC is decreased by addition of jasplakinolide, which induces actin filament polymerization, and conversely increased in response to the depolymerization of actin filaments by latrunculin B. To confirm the involvement of XSSH in this XAC dephosphorylation process, we immunodepleted XSSH from CSF extracts and examined changes in XAC phosphorylation states (Figure 4C). As shown in Figure 4C (top two), XSSH is effectively depleted, whereas almost the same amounts of actin remain in both mock- and XSSH-depleted extracts. Depletion of XSSH alone increases the amount of pXAC in the extract, suggesting that phosphorylation and dephosphorylation of XAC are dynamically maintained in CSF extracts. When this XSSH-depleted extract is treated with jasplakinolide to increase actin filaments, the XAC dephosphorylation is significantly inhibited. Conversely, treatment of the extract with latrunculin B leads to further phosphorylation of XAC. Therefore the results suggest that XSSH functions as an actin filament sensor to dephosphorylate XAC when the amount of actin filaments increases.

Low-speed extracts prepared from oocytes were ultracentrifuged to localize actin and XSSH (Figure 4D). In immature oocytes (control), unphosphorylated XSSH is present in both the supernatants and precipitates after ultracentrifugation (Figure 4D, top). Actin is also similarly present in both the supernatants and precipitates (Figure 4D, top), indicating that a significant amount of actin is sequestered from polymerization. On the other hand, in mature oocytes (control), in which XSSH was mostly phosphorylated, actin and XSSH are also present in both the supernatant and precipitate, but the hyperphosphorylated XSSH in the lower-mobility group is detected only in the supernatant after ultracentrifugation (Figure 4D, bottom). In both immature and matured oocytes treated with latrunculin B, the amount of sedimented XSSH apparently decreases to some extent after ultracentrifugation (Figure 4, D and F). Jasplakinolide-treatment increases actin in both low- and high-speed precipitates (Figure 4D), whereas, unexpectedly, the amount of XSSH in the precipitates of both immature and mature oocytes does not increase and instead decreases compared to control oocytes (Figure 4F). By using CSF extracts, we obtained the same results as described earlier. As shown in Figure 4, E and F, treatment of CSF extracts with latrunculin B apparently decreases the sedimented XSSH, whereas treating the extracts with jasplakinolide or phalloidin does not increase XSSH in the precipitate, although the two drugs increase actin filaments in high-speed precipitates. Hyperphosphorylated XSSH is still present in the high-speed supernatant. Together these results suggest that XSSH does not bind directly to jasplakinolide- or phalloidin-induced actin filaments and that a certain amount of XSSH is involved in XAC dephosphorylation by binding to actin filaments. The results also suggest that phosphorylated XSSH is present in the soluble cytoplasm to be sequestered from actin filaments.

Inhibition of XAC dephosphorylation and meiotic spindle formation by injection of anti-XSSH antibodies

To determine the role of XSSH during progression of oocyte maturation, we carried out injection of the anti-XSSH antibody (Figure 5). This antibody was obtained by immunizing rabbits with the phosphatase domain of XSSH and then was affinity purified (Tanaka *et al.*, 2005b). The specificity of this antibody was verified by Western blot

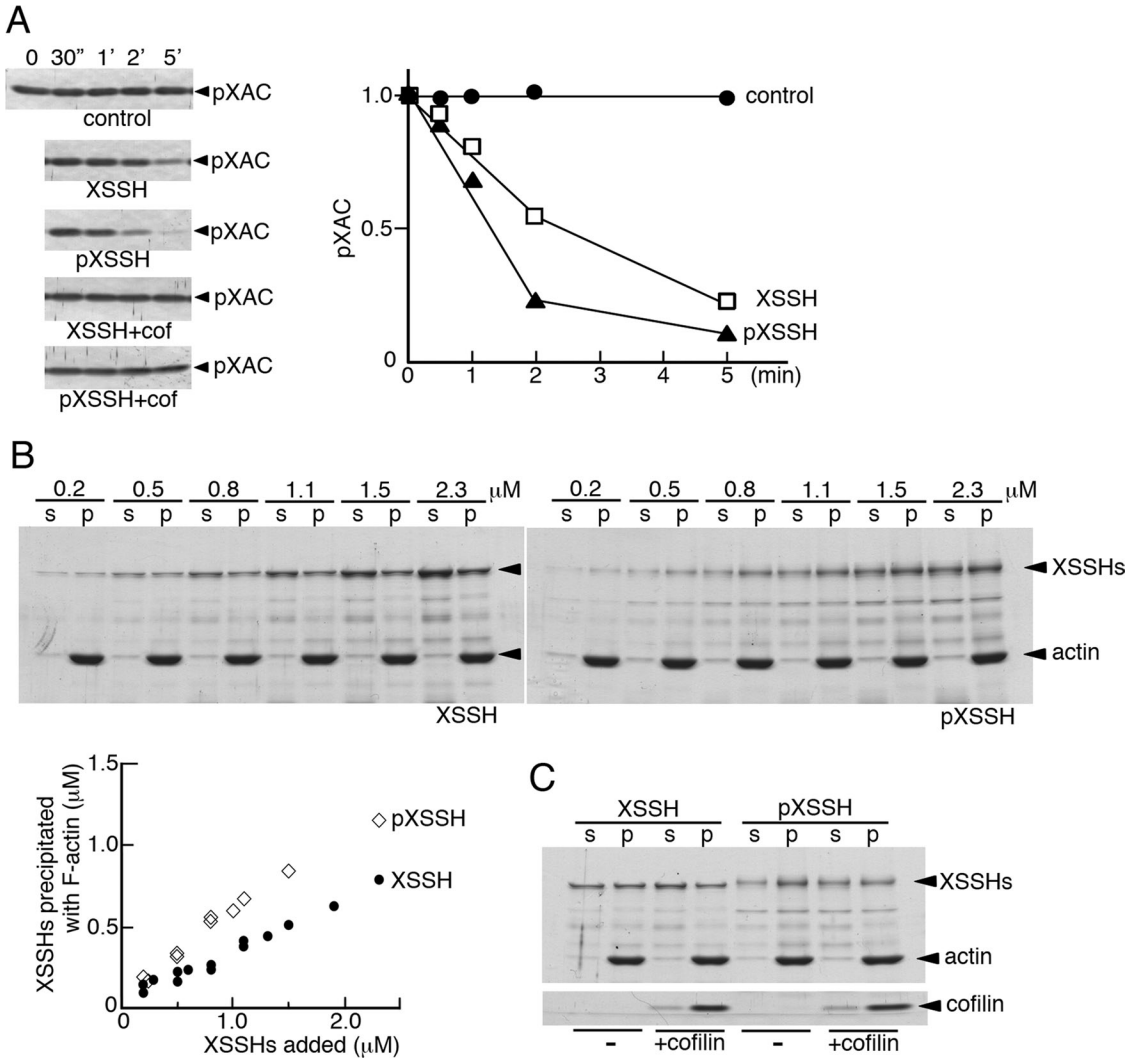

FIGURE 3: Effects of phosphorylation of XSSH on its phosphatase activity (A, D) and F-actin–binding ability (B, C) in vitro. (A) Time course of dephosphorylation of 10 μM pXAC by 0.2 μM XSSH in the absence of F-actin (control), 0.2 μM XSSH in the presence of 4.2 μM F-actin (XSSH), or 0.2 μM pXSSH in the presence of 4.2 μM F-actin (pXSSH). Dephosphorylation of pXAC was monitored by immunoblots using anti–phospho-ADF/cofilin antibody (top left, three). The results were quantified by densitometry and are shown as relative band intensity in the graph (1.0 at time 0). Bottom left two, time course of dephosphorylation of pXAC under the same conditions as described except for the presence of 4.7 μM chicken cofilin with 4.2 μM F-actin (XSSH+cof and pXSSH+cof). (B) Pelleting assay of XSSH (top) and pXSSH (bottom) with 4.7 μM F-actin by altering the concentrations of XSSH or pXSSH as indicated. Supernatants (s) and pellets (p) were examined by SDS–PAGE and Coomassie staining. The graph shows concentration of XSSHs in pellets vs. that of added XSSHs. The data from three independent experiments are plotted. (C) Pelleting assay of 1 μM XSSH or pXSSH with 4.7 μM F-actin in the presence (+cofilin) or absence (–) of 4.7 μM chick cofilin.

against CSF extracts (Supplemental Figure S2). Of interest, injection of purified anti-XSSH immunoglobulin G (IgG) into oocytes prevented the formation of white maturation spots (WMS) after progesterone treatment (Figure 5A). Nuclei in these oocytes disappeared, indicating that GVBD normally occurred (Figure 6). To clarify the effect of this antibody on the inhibition of WMS formation, we first analyzed the effect of this antibody on the phosphatase activity of XSSH. As shown in Figure 5B, dephosphorylation of XAC by GST-XSSH is not affected by the presence of the anti-XSSH IgG, indicating that this antibody does not inhibit directly phosphatase activity. In addition, this antibody does not directly activate XSSH by binding to it, since this antibody did not elevate phosphatase activity in the absence of actin filaments. In addition, this antibody is not likely to interfere with binding of XSSH to actin filaments, because phosphatase activity required interaction of XSSH with actin filaments. These results indicate that the anti-XSSH IgG does not directly affect XSSH activities.

We next examined phosphorylation states of XSSH in anti-XSSH–injected oocytes and found that the hyperphosphorylation of XSSH after GVBD was specifically suppressed in these oocytes (Figure 5C). Of interest, the XSSH bands in the antibody-injected oocytes were situated midway between the band in immature oocytes (nonphosphorylated XSSH) and that in control (matured) oocytes (hyperphosphorylated XSSH). Binding of the antibody to endogenous XSSH was confirmed by precipitation of XSSH when antibody-injected oocytes were homogenized in phosphate-buffered saline (PBS) and

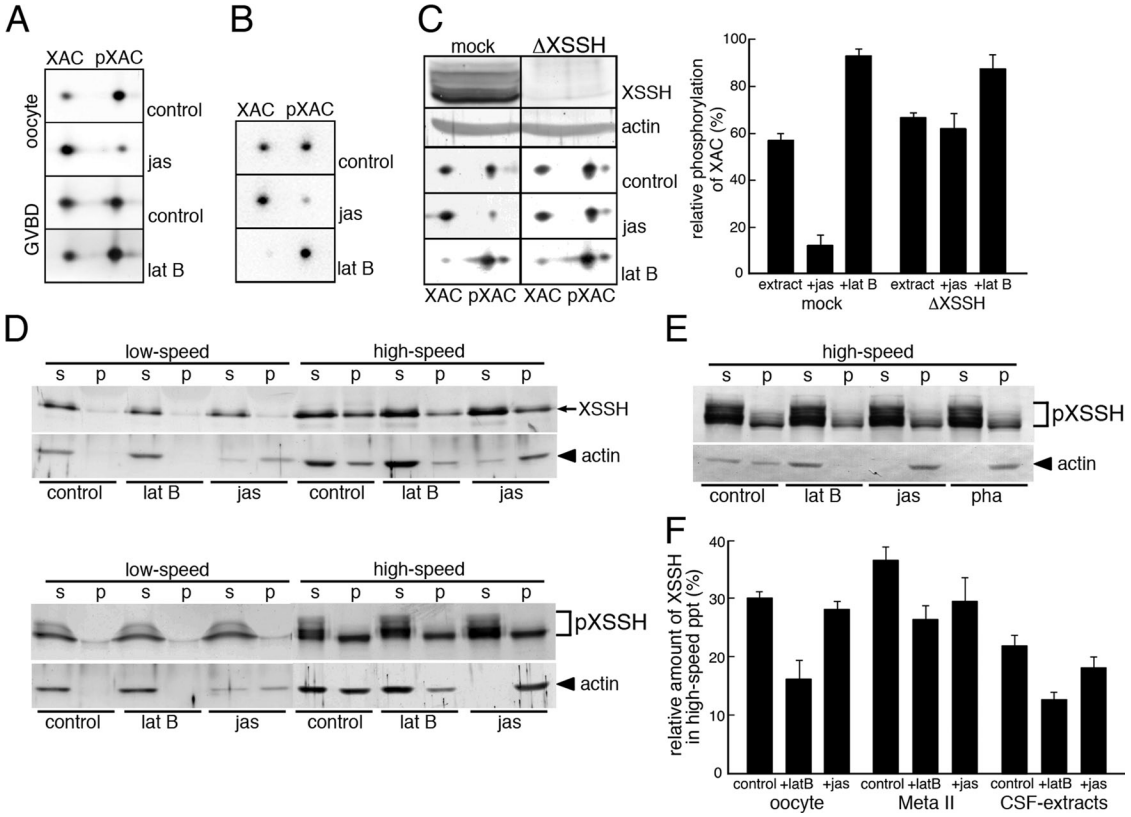

FIGURE 4: Effects of F-actin levels on the XAC phosphatase activity of XSSH. (A) Phosphorylation states of XAC were examined by 2D immunoblots of XAC in immature oocytes (oocyte) and maturing oocytes just after GVBD, which were treated with jasplakinolide (jas) or latrunculin B (lat B). Control indicates the treatment with vehicle alone. (B) Phosphorylation states of XAC were examined by 2D immunoblots of XAC in CSF extracts in the presence of jas or lat B. Control indicates addition of vehicle alone. (C) Phosphorylation states of XAC were examined by 2D immunoblots of XAC in mock-depleted CSF extracts (mock) or XSSH-depleted CSF extracts (ΔXSSH) in the absence (control) or presence of jas or lat B. XSSH was sufficiently depleted from CSF extracts (front row, XSSH) as judged by the anti-actin blots (second row, actin). The spots of XAC and pXAC were quantified by densitometry, and percentages of pXAC are shown. (D) Immature oocytes (top) and maturing oocytes just after GVBD (bottom) treated with vehicle alone (control), lat B, or jas were centrifuged at 12,000 × *g* for 15 min (low speed), and the supernatants were further ultracentrifuged at 436,000 × *g* for 20 min (high speed) to separate the supernatants and pellets. The supernatants (s) and pellets (p) were subjected to SDS–PAGE and examined by immunoblotting with anti-XSSH or anti-actin antibody. (E) Immunoblots of XSSH and actin in high-speed supernatants (s) and pellets (p) of CSF extracts treated with vehicle alone (control), 25 μM lat B, 10 μM jas, or 10 μM phalloidin (pha) as described in D. (F) The XSSH bands in high-speed supernatants and precipitates (ppt) were quantified by densitometry, and percentages of precipitated XSSH are shown. Bars, mean + SE from three independent experiments using immature oocytes (oocyte), mature oocytes (Meta II), and CSF extracts in the absence (control) or presence of latrunculin B (+latB) or jasplakinolide (+jas).

centrifuged (Figure 5D). These results show that XSSH was partially phosphorylated but not fully phosphorylated due to binding of the antibody to XSSH. Examination of the phosphorylation state of XAC in antibody-injected oocytes revealed that dephosphorylation of XAC was suppressed (Figure 5E). Furthermore, coinjection of constitutively active chicken cofilin (S3A-cof) restored the WMS formation (Figure 5A) without affecting the pXAC level (Figure 5E), whereas the phosphomimetic inactive form of cofilin (S3D-cof) did not restore the WMS formation (Figure 5A). On the other hand, phosphorylatable wild-type cofilin could restore the WMS formation, but its effect was weaker than that of S3A-cofilin. Together these data strongly suggest that XAC activation occurs downstream of XSSH phosphorylation and that inhibition of XSSH hyperphosphorylation by antibody injection suppresses WMS formation due to failure of XAC dephosphorylation.

We observed cytological structures in the antibody-injected oocytes and found that formation of the meiotic spindle was inhibited (Figure 6). When control oocytes just formed WMS, the MTOC-TMA complex was formed at the vegetal portion of breaking GV and migrated toward the animal pole (Figure 6A). In anti-XSSH–injected oocytes, however, the MTOC-TMA complex poorly formed at either vegetal or animal portion of GV, indicating that the concentration of MTOC to the vegetal side of GV is inhibited. The yolk-free region formed at the vegetal part of the cytoplasm beneath GV showed a broader and irregular shape (Figure 6B). In addition, the MTOC-TMA complex disappeared from the yolk-free region after completion of GVBD (Figure 6B). At 4 h after the WMS formation, control oocytes formed meiotic spindles at animal cortices (Figure 6C). In antibody-injected oocytes, the yolk-free region formed by GVBD remained and was scattered by fine, radial microtubule structures (Figure 6D). These atypical microtubule structures were not observed in normal oocytes just after GVBD, at which the typical yolk-free region appeared. These results indicate that full phosphorylation (hyperphosphorylation) of XSSH is required for progression of

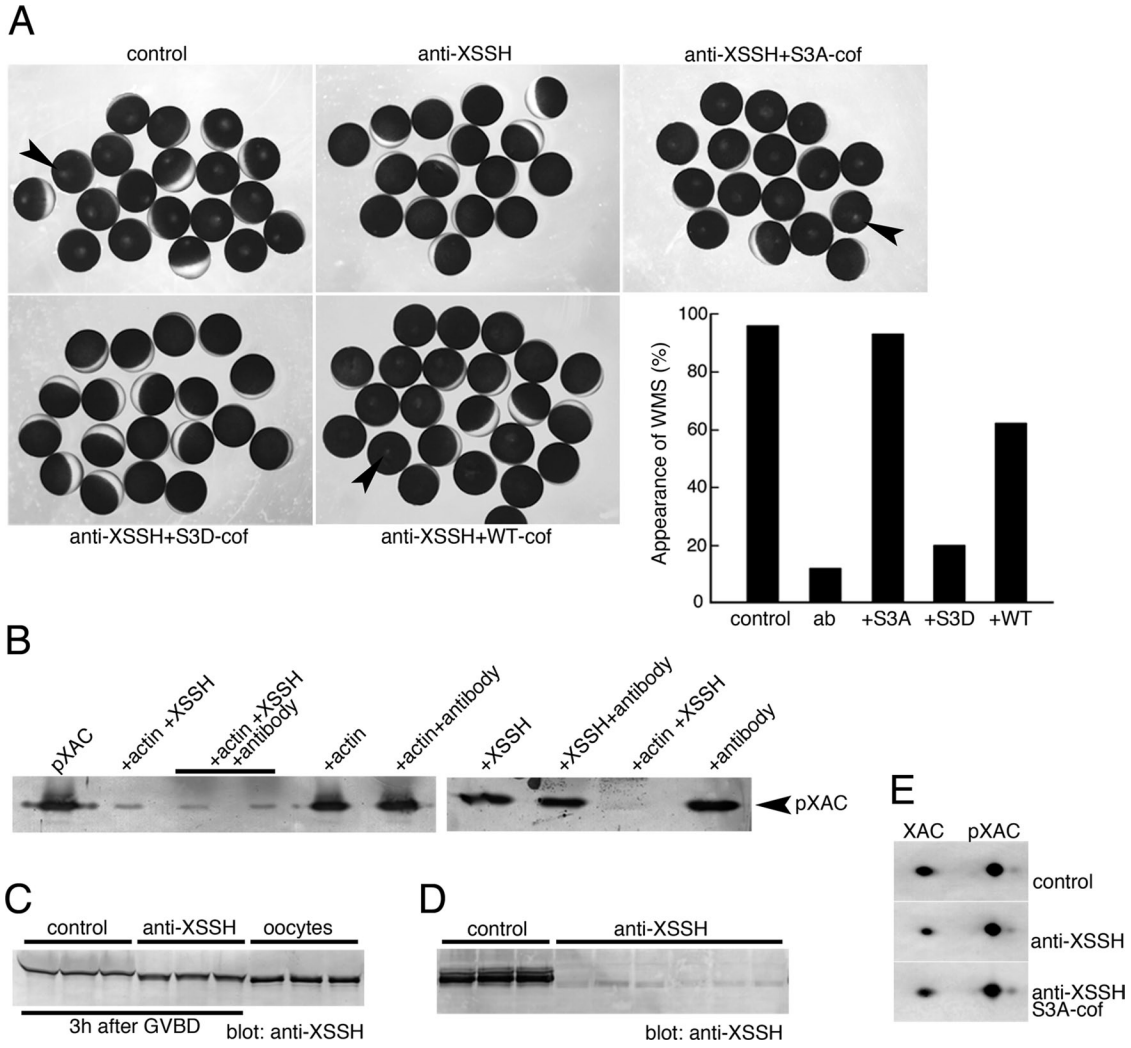

FIGURE 5: Effects of the anti-XSSH antibody on the XSSH activity in vitro and the phosphorylation states of XSSH and XAC in maturing oocytes. (A) *Xenopus* oocytes were injected with buffer alone (control), anti-XSSH, anti-XSSH plus constitutively active cofilin (S3A-cof), anti-XSSH plus phosphomimetic inactive cofilin (S3D-cof), or anti-XSSH plus wild-type cofilin (WT-cof). The concentrations of anti-XSSH IgG and cofilins were 8 and 0.5 mg/ml, respectively. After progesterone treatment, WMS formation (indicated by arrowheads) was examined. A typical example of injection experiments is summarized in the graph. ab, anti-XSSH antibody injection. (B) Effect of the anti-XSSH antibody on the XAC phosphatase activity of XSSH was examined by incubating pXAC (left lane) with combinations of 4.7 μM F-actin, 0.3 μM XSSH, and 1 mg/ml antibody as indicated, followed by immunoblot with anti–phospho-ADF/cofilin antibody. pXAC was dephosphorylated in the presence of F-actin and XSSH, and addition of anti-XSSH antibody did not inhibit dephosphorylation. Actin alone, antibody alone, XSSH alone, or actin and the antibody without XSSH did not alter pXAC dephosphorylation. The anti-XSSH antibody did not activate XSSH in the absence of F-actin. (C) Effects of anti-XSSH antibody on phosphorylation of XSSH in oocytes. Oocytes were injected with buffer alone (control; three samples) or anti-XSSH antibody (three samples) and examined at 3 h after GVBD by immunoblot with anti-XSSH antibody. Right, three samples of untreated immature oocytes as controls to determine mobility of nonphosphorylated XSSH. Injection of anti-XSSH antibody partially inhibited full phosphorylation of XSSH during oocyte maturation. (D) Binding of the anti-XSSH antibody to XSSH in mature oocytes. Control and antibody-injected oocytes were homogenized with PBS and centrifuged (at low speed). The supernatants were subjected to SDS–PAGE and immunoblotting with anti-XSSH antibody. Three control and six antibody-injected samples are shown. (E) Effects of the anti-XSSH antibody on the phosphorylation states of XAC during oocyte maturation. Oocytes were injected with buffer alone (control), anti-XSSH antibody, or anti-XSSH antibody and S3A-cofilin and examined by 2D immunoblot with anti-XAC antibody, when >80% of control oocytes show WMS.

meiotic spindle formation after GVBD. Because full phosphorylation of XSSH correlates with XAC dephosphorylation as mentioned, actin dynamics might be critical for meiotic spindle assembly. To clarify this point, we treated oocytes with jasplakinolide to stabilize actin filaments and examined its effect on spindle formation (Figure 6E). As previously shown (Okada *et al.*, 2012), jasplakinolide treatment induced the formation of thick actin layer at the oocyte cortex (Figure 6F). In these oocytes, fine, radial microtubule structures were also scattered in the cytoplasm, which resembled structures formed in anti-XSSH-antibody–injected oocytes. Thus the results strongly suggest that spindle formation requires actin dynamics in *Xenopus* oocytes.

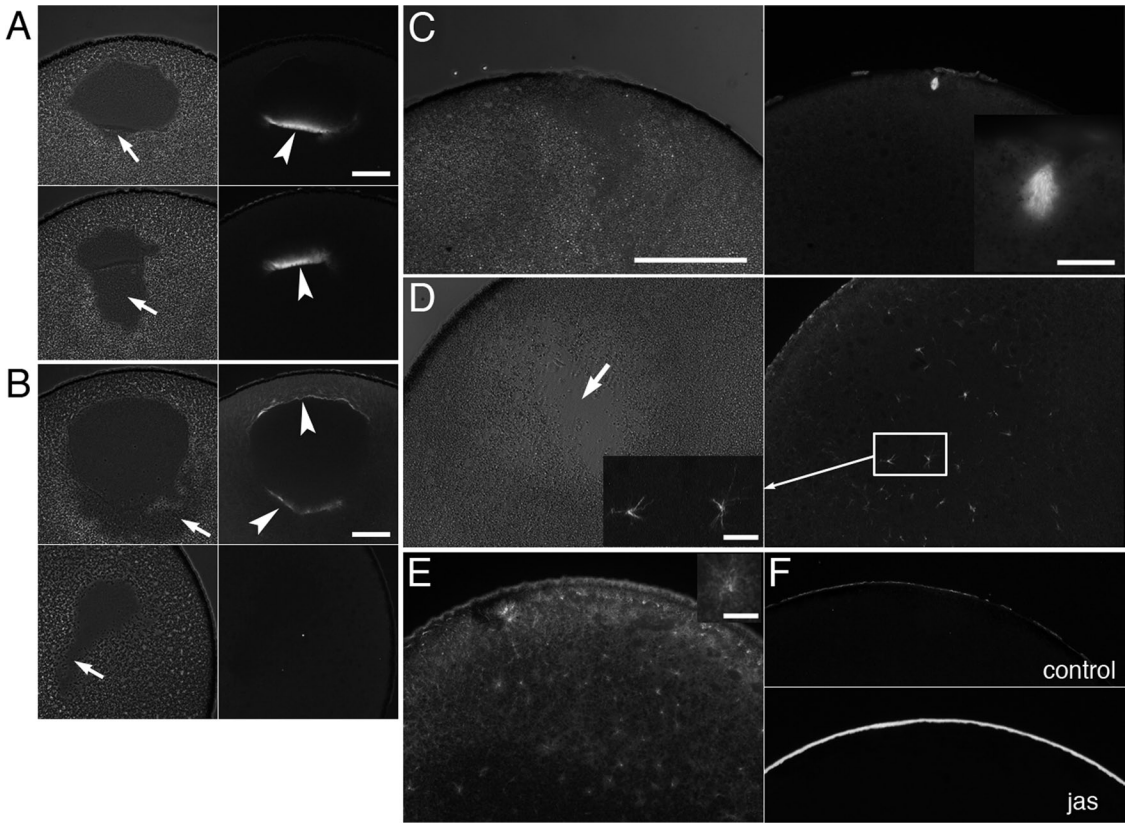

FIGURE 6: Effects of injection of anti-XSSH antibody on assembly of MTOC-TMA and meiotic spindles. (A, B) Phase contrast (left) and immunofluorescence (right) microscopy of control oocytes injected with buffer alone (A) or oocytes injected with anti-XSSH antibody (B). Microtubules were stained with anti-tubulin antibody (right). Assembly of MTOC-TMA (arrowhead in A, top right) at the basal region of GV and its migration toward the animal pole (arrowhead in A, bottom right) are clearly visible in control (A), whereas its structure is faint in antibody-injected oocytes (arrowheads in B, top right). The yolk-free region formed at the basal region of GV (indicated by arrows in phase contrast micrographs) showed broader and irregular shape in anti-XSSH antibody-injected oocytes (B). (C, D) Phase contrast images (left) and immunofluorescence staining for tubulin (right) of control oocytes 4 h after GVBD (C) and antibody-injected oocytes fixed at 4 h after control oocytes formed WMS (D). Meiotic spindles were already assembled in control oocytes (C, magnified in inset), whereas fine and radial microtubule structures were formed (D, left, magnified) and scattered around the yolk-free region in antibody-injected oocytes (D, arrow). (E) A jasplakinolide-treated oocyte was fixed at 4 h after control oocytes formed WMS and stained with anti-tubulin antibody. An example of radial microtubule structures is shown in the inset on the upper right corner. (F) Staining of control (top) and jasplakinolide-treated (bottom) oocytes for actin filaments by anti-actin antibody. Note the cortical accumulation of actin filaments by jasplakinolide treatment. Bars, (A, B) 100 μm, (C, applies to C– F) 200 μm, (insets) 20 μm.

DISCUSSION

In this study, we demonstrated that hyperphosphorylation of XSSH correlated with XAC dephosphorylation and that anti-XSSH IgG, which suppressed hyperphosphorylation of XSSH after GVBD, inhibited both XAC dephosphorylation and meiotic spindle assembly. This spindle defect was restored by constitutively active cofilin but not by an inactive form of cofilin, indicating that XAC activity was essential for the spindle assembly. The recovery effect by wild-type cofilin may be due to increasing amount of cofilin, which is not phosphorylated in oocytes. Jasplakinolide stabilized cortical actin filaments and impeded spindle assembly, supporting the significance of actin dynamics for spindle assembly. Together the results indicate that meiotic spindle assembly may require XAC-mediated actin filament dynamics that is controlled through XSSH regulation via phosphorylation. The functional significance of cytoplasmic and cortical actin filaments during oocyte maturation is beginning to be understood (for reviews see Field and Lénárt, 2011; Sandquist *et al.*, 2011; Verlhac, 2011). In murine oocytes, however, actin filaments are required for meiotic spindle migration and anchoring but are not involved in spindle assembly during maturation. The present study in *Xenopus* oocytes contrasts with these reports. Previously, actin filaments were reported to be associated with meiotic spindles in *Xenopus* oocytes (Weber *et al.*, 2004). Disruption of myosin X, which binds to both actin filaments and microtubules, causes the formation of actin aggregates and malformation of meiotic spindles, suggesting a direct functional link between actin filaments and spindle formation. Thus we propose a novel regulatory link between actin filament dynamics and meiotic spindle formation during *Xenopus* oocyte maturation.

How are actin dynamics involved in spindle assembly? One possible explanation is that stabilized actin filaments disrupt proper MTOC assembly and subsequent formation of meiotic spindles. During oocyte maturation, MTOC is initially translocated at the basal part of the GV before GVBD to induce the formation of the MTOC-TMA complex, and then its migration toward the animal cortex begins shortly after GVBD (Gard, 1992; Gard *et al.*, 1995;

Becker *et al.*, 2003). The MTOC-TMA complex serves as the immediate precursor of the first meiotic spindle by forming a compact aggregate of microtubules and chromosomes (Gard, 1992). The present study strongly suggests functional correlation between XAC activation and MTOC-TMA assembly; antibody injection inhibited XAC dephosphorylation and assembly of MTOC at the vegetal portion of GV and subsequent assembly of the MTOC-TMA complex (Figure 5B).

Pioneering work by Gard *et al*. (1995) demonstrated that treatment of oocytes with cytochalasin B during maturation disrupted the normal organization of the MTOC-TMA complex; it appeared broader than that formed in normal oocytes and sometimes appeared to be split into two or more fragments in cytochalasin B–treated oocytes. Of interest, this drug never blocked assembly of meiotic spindles. The present study, however, demonstrated that anti-XSSH IgG injection and jasplakinolide treatment inhibited spindle assembly. In addition, phalloidin injection induced atypical formation of radial microtubule arrays in the cytoplasm apart from the nucleus and prevented the formation of MTOC-TMA at the basal part of the remaining nucleus (Okada *et al.*, 2012). These differences in spindle assembly may be partly due to opposite effects of the drugs and antibody on actin filament dynamics. The total amount of actin filaments is reduced in cytochalasin B–treated oocytes because cytochalasin B blocks monomer addition at the barbed ends of actin filaments to inhibit actin filament assembly. In contrast, phalloidin and jasplakinolide stabilize actin filaments to increase the total amount of actin filaments and prevent actin filaments from effects of XAC-induced dynamics in oocytes (Okada *et al*., 2012). The inhibition of XAC dephosphorylation (activation) by antibody injection may also produce similar effects on actin dynamics to jasplakinolide and phalloidin treatment because XAC-driven actin filament reorganization is suppressed in both antibody-injected and jasplakinolide-treated oocytes. We assume that a decrease in actin filament turnover impedes correct localization of MTOC to the basal part of the nucleus to lead to malformation of the MTOC-TMA complex. This assumption is supported by a previous finding that normal formation of MTOC-TMA is disrupted in oocytes injected with constitutively active LIM kinases (Takahashi *et al.*, 2001). The defect of MTOC-TMA might be derived from kinase action, which decreases actin dynamics by phosphorylation and inactivation of XAC, although the effect of LIM kinases on spindle assembly remains to be clarified. On the other hand, spindle assembly may require dynamic reorganization of preexisting actin filaments rather than increase in actin turnover rate, since an excess amount of stabilized actin filaments inhibited spindle assembly. The behavior of MTOC should be examined in antibody-injected oocytes by visualizing MTOC components in future studies.

We demonstrated that hyperphosphorylation of the XSSH tail domain occurs just after GVBD. The phosphorylation sites were concentrated in the tail domain, especially at the N-tail region. Fourteen sites were identified in the N-tail region, and additional unidentified sites should be present in the C-tail regions. Mammalian SSH is negatively regulated by phosphorylation, and the phosphorylated tail domain associates with the 14-3-3 family of proteins, which inhibits association of XSSH with actin filaments, indicating that phosphorylation inactivates SSH (e.g., Nagata-Ohashi *et al.*, 2004; Soosairajah *et al.*, 2005; Kligys *et al.*, 2007; Eiseler *et al.*, 2009). Our results on *Xenopus* SSH are quite different from those reported for mammalian SSH. In particular, phosphorylation of mammalian SSH is sufficient to inhibit its phosphatase activity (Soosairajah *et al.*, 2005). In contrast, hyperphosphorylation of XSSH at the tail domain did not inhibit phosphatase activity in vitro. It was reported that phosphorylation of the Ser residue in the dual-specific phosphatase catalytic (DSPc) domain of SSH inhibits its phosphatase activity (Soosairajah *et al.*, 2005; Barišič *et al.*, 2011). In the present study, however, in vitro phosphatase assay did not show suppression of XSSH activity by phosphorylation, or rather, the activity was enhanced by phosphorylation. Thus negative regulation via phosphorylation of DSPc domain is not the case in *Xenopus* oocytes. We found the phosphorylation consensus sequence, LMRSIS, for PKD1 (Eiseler *et al*., 2009; Barišič *et al.*, 2011) in the N-tail region. This sequence, when phosphorylated, matches a 14-3-3–binding motif (Eiseler *et al*., 2009). CSF extracts indeed phosphorylated this site, but we could detect binding of 14-3-3ζ neither to this site nor other sites in the phosphorylated N-tail region. Furthermore, our finding that 14-3-3ζ bound to both unphosphorylated and phosphorylated C-tail region suggests that the involvement of 14-3-3 in the XSSH-regulatory system is complicated. Hyperphosphorylation of the tail domain may provide some scaffolds for a certain protein other than 14-3-3, or the cloud of negative charge formed in the tail domain may cause electrostatic interactions with other cellular components. Further studies are required to understand how hyperphosphorylation regulates XSSH activity in *Xenopus* oocytes.

It is of interest to note that changes in the amount of actin filaments regulate the phosphorylation state of XAC. In immature oocytes, in which XSSH is unphosphorylated and most XAC is phosphorylated, jasplakinolide treatment caused a drastic increase in dephosphorylated XAC level. On the other hand, in mature oocytes, in which all XSSH was phosphorylated and about one-half of XAC was dephosphorylated, latrunculin B suppressed the increase in dephosphorylated XAC level. CSF extracts, a model system for mature oocytes, also retained sensitivity to F-actin levels, and, further, immunodepletion of XSSH inhibited jasplakinolide-induced XAC dephosphorylation. These results indicate that dephosphorylation of XAC induced by jasplakinolide is dependent on XSSH activity but independent of the phosphorylation state of XSSH, that is, both phosphorylated and unphosphorylated forms of XSSH can dephosphorylate XAC in response to F-actin content.

Then, how do XSSH and XAC regulate the actin filament dynamics in oocytes? It is widely recognized that intracellular actin filament assembly and disassembly are dynamically regulated (Pollard and Cooper, 2009). Because XAC is a key regulator of actin dynamics, its phosphorylation levels directly affect actin filament dynamics. Thus the experimentally obtained ratio of phosphorylated and dephosphorylated XAC might reflect catalytic equilibrium between phosphorylation and dephosphorylation of XAC. Our results from XSSH-depletion experiments provide evidence for dynamic regulation by phosphorylation (Figure 4C). If depolymerization of actin filaments only suppresses XSSH activation, the phosphorylation level of XAC in XSSH-depleted extracts would not be altered before and after latrunculin B treatment, but this was not the case in depleted extracts. Both latrunculin B treatment and XSSH depletion increased phosphorylated XAC level above control due to reduced XSSH activity. However, when the XSSH-depleted extracts were treated with latrunculin B, the phosphorylated XAC level, which had been already increased by XSSH depletion. was further elevated. These results indicate that a kinase for XAC (probably LIM kinases) competes continuously with XSSH action, and, of interest, that actin filaments should negatively regulate the kinase. Actin filament–dependent regulation of actin dynamics can be modeled as follows. XSSH is activated by binding to actin filaments and dephosphorylates XAC. The activated XAC depolymerizes actin filaments. In addition, XAC weakly competes with XSSH for binding to actin filaments (Figure 3C). Dissociation of XSSH from actin filaments causes

reduction in its phosphatase activity. Decrease in the amount of actin filaments also suppresses F-actin–dependent inhibition of the XAC kinase to accelerate phosphorylation. The active XAC kinase phosphorylates XAC to lead to polymerization of actin filaments. Thus a certain amount of actin filaments can be dynamically maintained.

Hyperphosphorylation of XSSH occurred drastically just after GVBD and was accompanied by dephosphorylation of XAC. This suggests that XSSH hyperphosphorylation and subsequent XAC dephosphorylation alter the steady-state actin dynamics maintained in immature oocytes. However, one puzzling result is that the hyperphosphorylated XSSH in the lower-mobility group remained soluble in the cytoplasm and was apparently dissociated from actin filaments (Figure 4). This is inconsistent with a simple model that hyperphosphorylation of XSSH leads to dephosphorylation of XAC. It should be noted, however, that the higher-mobility group could cosediment with actin filaments. From these results, we postulate that phosphorylation of XSSH is dually regulated: hyperphosphorylation leads to inhibition of its binding to actin filaments. but the lower level of phosphorylation does not. During oocyte maturation, GVBD occurs when MPF activity is sufficiently increased. The timing of XSSH phosphorylation is just after GVBD, and MPF activity that maintains the meiotic phase is constantly kept highest, at least until first meiotic spindle assembly. Under these intracellular conditions, XSSH would be fully phosphorylated but the phosphorylation level would actually be different. In addition, whereas XSSH hyperphosphorylation drastically occurs just after GVBD, the subsequent XAC dephosphorylation level gradually increases until complete maturation. This suggests the presence of a fine regulatory system for XAC dephosphorylation. We found an additional band with the lowest mobility, which was further hyperphosphorylated by adding okadaic acid to the CSF extracts (Figure 2D). This indicates the phosphorylation level of XSSH is dynamically regulated, at least in part, by type 1 and/or type 2A phosphatases as being antagonistic to XSSH kinases. The significance of regulation by phosphorylation is also provided by anti-XSSH IgG injection experiments. The hyperphosphorylation of XSSH was partially inhibited by the injection of anti-XSSH IgG. Then, dephosphorylation of XAC was strongly inhibited. This partial inhibition of XSSH phosphorylation might negatively affect XAC dephosphorylation. This partial phosphorylation state may be maintained by binding of the antibody to the phosphatase domain of XSSH. Thus accessibility of kinases and phosphatases for XSSH might be restricted due to steric hindrance by binding of antibody. Because N-tail was scarcely phosphorylated at interphase, hyperphosphorylation occurred specifically at meiotic phase. We assume that, under the conditions that phosphorylation by MPF and its downstream kinases predominate, local regulation of hyperphosphorylated XSSH by dephosphorylation may be required for actin filament dynamics.

In mouse oocytes, actin filaments are not involved in spindle assembly (Longo and Chen, 1985; Verlhac *et al.*, 2000; Liu *et al.*, 2002; Calarco, 2005). On the other hand, a three-dimensional actin meshwork formed after GVBD in the nuclear region is required for chromosome congression in starfish oocytes (Lénárt *et al.*, 2005). The difference of requirement of actin filaments for spindle assembly during oocyte maturation is believed to be due to the cell size. Microtubule-based mechanisms required for spindle assembly may be insufficient to capture chromosomes scattered in the large nucleus of starfish oocytes (Field and Lénárt, 2011). Actin filaments, which are absent in Pro I nuclei of starfish oocytes, rapidly assemble just after GVBD in the nuclear region. In *Xenopus* oocytes, however, a dense actin filament meshwork is reported to be already present in nuclei of Pro I oocytes (Bohnsack *et al.*, 2006; Miyamoto *et al.*, 2011). The actin meshwork that spans the entire nucleus might mechanically support the extremely large oocyte nucleus (Bohnsack *et al.*, 2006) and also capture chromosomes. To undergo proper congression of chromosomes and subsequent spindle assembly, XAC may contribute to meshwork reorganization through regulation of XSSH by phosphorylation just after GVBD.

MATERIALS AND METHODS

Oocyte preparation and culture

Female *X. laevis* were anesthetized in ice water, and lobes of ovaries were excised from a small incision made in the posterior ventral side. Oocytes were obtained by manual defolliculation with watchmaker's forceps and maintained in OR2 medium (82.5 mM NaCl, 2.5 mM KCl, 1 mM $CaCl_2$, 1 mM $MgCl_2$, 1 mM Na_2HPO_4, 5 mM 4-(2-hydroxyethyl)-1-piperazineethanesulfonic acid [HEPES]-NaOH, pH 7.8) at 16°C in agarose-coated plastic dishes. For in vitro maturation, defolliculated stage VI oocytes were incubated in OR2 medium containing 5 µM progesterone at 19°C until GVBD as indicated by the appearance of the WMS. Thereafter, oocytes were further incubated in OR2 medium at the times indicated. To alter the F-actin content in oocytes, immature oocytes were incubated in OR2 medium containing jasplakinolide for 1 h or OR2 medium containing 5 µM progesterone and 25 µM latrunculin B or 10 µM jasplakinolide for periods required for oocyte maturation.

To monitor the progression of oocyte maturation until WMS formation, since the timing of GVBD after progesterone exposure varied widely among oocytes, we used relative time points; 0 is specified when immature oocytes are added with progesterone, and 1.0 is when >80% oocytes show WMS. To obtain oocytes that just had GVBD, the oocytes that just formed WMS were collected under a dissection microscope.

Preparation of oocyte and egg extracts

CSF extracts were prepared from unfertilized eggs as described by Murray (1991), in the absence of cytochalasin B. Interphase extracts and reentered mitotic extracts (prepared by adding ΔN85 cyclin B2 to interphase extracts) were prepared according to Glotzer *et al.* (1991).

For SDS–PAGE, one oocyte was crushed by sonication in 20 µl of yolk-removing buffer (0.1 M NaCl, 2 mM ethylene glycol tetraacetic acid [EGTA], 1% Triton X-100, 0.05% SDS, 1 mM phenylmethylsulfonyl fluoride, and 20 mM Na-PO_4 buffer, pH 7.0). After centrifugation at 13,000 rpm for 15 min, the supernatant was mixed with the same volume of SDS-sample buffer. For monitoring F-actin content, immature or mature oocytes were homogenized in CSF-XB (100 mM KCl, 0.1 mM $CaCl_2$, 2 mM $MgCl_2$, 5 mM EGTA, 7.5 mM creatine phosphate, 20 mM ATP, 50 mM sucrose, and 10 mM HEPES-KOH, pH 7.7) containing 10 µg/ml leupeptin, chymostatin, and pepstatin and centrifuged at 13,000 rpm for 15 min. The supernatants were further ultracentrifuged at 436,000 × *g* for 20 min. The supernatants and pellets were subjected to SDS–PAGE and immunoblotting.

PAGE and immunoblotting

SDS–PAGE was carried out according to Laemmli (1970). Two-dimensional gel electrophoresis (2D-PAGE) was performed according to O'Farrell *et al.* (1977) using nonequilibrium-pH-gradient gel electrophoresis for the first dimension. Several oocytes were homogenized by sonication directly in 150 µl of SDS-sample buffer (4% SDS, 10% 2-mercaptethanol, 20% glycerol, and 50 mM Tris-HCl, pH 7.0) to avoid dephosphorylation of XAC. Proteins

were precipitated by methanol/chloroform (Wessel and Flugge, 1984), dried, and dissolved in 2D-PAGE buffer composed of 9 M urea, 2% ampholine, pH 3.5–10, 5% 2-mercaptoethanol, 0.1% SDS, 1% NP-40, and 10 mM Tris-HCl, pH 7.5. For immunoblotting, proteins were electrophoretically transferred from the SDS-gel to nitrocellulose membranes by the method of Towbin *et al.* (1979). The membranes were treated with 5% skimmed milk in PBS for 1 h and then incubated with the primary antibody, followed by treatment with alkaline phosphatase–conjugated secondary antibody. The paper was thoroughly washed with PBS after each immunoreaction and stained with nitroblue tetrazolium chloride and 5-bromo-4-chloro-3-indolylphosphate *p*-toluidine salt in alkaline phosphatase buffer (0.1 M NaCl, 5 mM $MgCl_2$, and 0.1 M Tris-HCl, pH 9.5). Quantification was carried out by densitometry with ImageJ (National Institutes of Health, Bethesda, MD).

Antibodies

Rabbit polyclonal anti-XSSH IgG for microinjection was prepared as described previously (Tanaka *et al.*, 2005b). To examine the antibody-injected oocytes by immunoblotting, we produced anti-XSSH antibody by immunizing GST-tail to guinea pigs. Anti-XAC monoclonal antibody was previously prepared (Okada *et al.*, 1999). Polyclonal antibody specific for phosphorylated ADF/cofilin was kindly provided by J. Bamburg (Colorado State University, Fort Collins, CO; Meberg *et al.*, 1998). Anti-actin polyclonal antibody was kindly provided by K. Iida (Tokyo Metropolitan Institute of Medical Science, Tokyo, Japan; Iida and Yahara, 1986). Monoclonal and polyclonal antibodies against tubulin (DM1A) and 14-3-3 proteins were purchased from Sigma-Aldrich (St. Louis, MO) and Santa Cruz Biotechnology (Santa Cruz, CA), respectively. Fluorescein-labeled goat anti-mouse or rabbit IgG was purchased from Tago (Burlingame, CA). Alkaline phosphatase–conjugated goat anti-mouse, rabbit, and guinea pig IgG were purchased from Bio-Rad (Hercules, CA) and Chemicon (Temecula, CA).

DNA constructs

Expression vectors for GST-fused XSSH variants, pGEX-XSSH, pGEX-AB, pGEX-Δtail, and pGEX-tail, were previously described (Tanaka *et al.*, 2005b). For GST-N-tail, pGEX-tail was mutagenized to introduce the *Eco*RI site and stop codon by substitution of T^{1607}, A^{1610}, and G^{1611} to G, T, and T using a QuikChange Mutagenesis Kit (Stratagene, Santa Clara, CA) with 5′-GTATTAGAAGAGACCACTTGAATTCAGAACTTTAATGTGTTAG and 5′-CTAACACATTAAAGTTCTGAATTCAAGTGGTCTCTTCTAATA as primers. For GST-C-tail, pGEX-N-tail was digested with *Eco*RI, and the fragment was inserted into the *Eco*RI site of pGEX-4T-2 vector. *Xenopus* 14-3-3ζ cDNA was obtained from the *Xenopus* ovary cDNA library by PCR with a primer set of 5′-ACCATGGATAAAAATGAACTGGTC and 5′-TTAGTTCTCCCCTCCTTCTCC. The amplified fragments were cloned into the pBluescript II vector at the *Eco*RV site and the sequences confirmed by DNA sequencing. For protein expression, 14-3-3ζ cDNA was excised out by digestion with *Eco*RI and *Xho*I and ligated into the same sites of the pGEX-4T-1 vector. pGEX-ΔN85 cyclin B2 was kindly provided by T. Kishimoto (Tokyo Institute of Technology, Tokyo, Japan). The mutagenesis procedure of phosphorylation-site mutants of GST-N-tail is given in the Supplemental Information.

Preparation of proteins

GST-XSSH and its truncated mutants and phosphorylated XAC fraction were prepared as described (Tanaka *et al.*, 2005b). GST–N-tail and GST–C-tail were prepared using glutathione–Sepharose 4B (GE Healthcare, Piscataway, NJ) according to the manufacturer's protocol. XAC was prepared as described (Okada *et al.*, 2012). 14-3-3ζ was expressed as a GST-fusion protein, bound to glutathione beads, and eluted from the column by digestion with thrombin, which was immobilized to *p*-aminobenzamidine-agarose. Actin was prepared from rabbit skeletal muscle by the method of Spudich and Watt (1971) and purified by gel filtration on a Sephadex G-200 column as described previously (Okada *et al.*, 1999). Wild-type and mutant chick cofilin were prepared as described (Nagaoka *et al.*, 1995, 1996).

Phosphorylation of XSSH in vitro

GST-XSSH and its truncated mutants were phosphorylated in CSF extracts. Two microliters of GST-fusion proteins (1 mg/ml) was added to 20 μl of CSF extracts and incubated for 1 h at 22°C. A 10-μl amount of glutathione–Sepharose 4B beads (GE Healthcare) equilibrated with CSF-XB was added to the mixture and incubated for 1 h at 4°C with gentle stirring to absorb GST-fusion proteins to the beads. Then beads were thoroughly washed with PBS containing 0.1% Triton X-100 and mixed with 100 μl of SDS-sample buffer. For alkaline phosphatase treatment, the beads after washing with PBS were incubated with 2 U of alkaline phosphatase in 20 μl of 0.1 M NaCl, 2 mM $MgCl_2$, and 50 mM Tris-HCl, pH 8.0, at 22°C for 1 h. After washing with PBS, the beads were treated with SDS-sample buffer as described.

For preparation of pXSSH for phosphatase and sedimentation assays, 500 μl of GST-XSSH–bound glutathione beads, as prepared in the GST-XSSH purification, was mixed with 1 ml of CSF extracts in the presence of 25 μM latrunculin B and 10 μM cytochalasin B to avoid the formation of aggregates during incubation. After 3 h at 22°C with gentle stirring, beads were thoroughly washed with PBS containing 0.1% Triton X-100. pXSSH was eluted from the beads by 20 mM glutathione and dialyzed to F-buffer (0.1 M KCl, 2 mM $MgCl_2$, 1 mM dithiothreitol [DTT], 0.01% NaN_3, and 20 mM HEPES-KOH, pH 7.2).

LC-MS/MS analysis

The gel slices were washed with water, followed by acetonitrile/water (1/1, vol/vol) and acetonitrile, and then vacuum dried. The dried gel slices were reswollen in 10% acetonitrile and 50 mM ammonium bicarbonate (pH 8) containing 0.1 μg of sequencing-grade modified trypsin (Promega, Madison, WI). Digestion was allowed to proceed overnight at 37°C. After digestion, the peptide mixtures were split into two equal parts and vacuum dried. One part was used to enrich for phosphopeptides using TiO_2 Mag Sepharose beads (GE Healthcare) according to the manufacturer's protocol. After enrichment, the peptides were again vacuum dried.

Both peptide mixtures were redissolved in 20 μl of 2% acetonitrile and 0.1% trifluoroacetic acid and analyzed on an Ultimate 3000 HPLC system (Dionex, Amsterdam, Netherlands) in-line connected to an LTQ Orbitrap XL mass spectrometer (Thermo Electron, Bremen, Germany). A 30-min gradient of 2 to 50% acetonitrile was followed by a washing and reequilibration step on an in-house–packed 15-cm-long, 75-μm–inner diameter column (Reprosil-Pur Basic C18-HD 3 μm; Dr. Maisch, Ammerbuch-Entringen, Germany). Per LC-MS/MS analysis, 5 μl of the peptide mixture was consumed. Instrument settings for LC-MS/MS analysis and the generation of MS/MS peak lists were as previously described (Ghesquière *et al.*, 2009).

These MS/MS peak lists were then searched using the Mascot Daemon interface (version 2.2.0; Matrix Science, London, United Kingdom). The Mascot search parameters were as follows. The spectra were searched in the human subsection of the Swiss-Prot

database to which the sequence of the Slingshot protein was added. This approach was used to create a large enough background of protein sequences for statistically solid matching of MS/MS spectra to the Slingshot protein sequence. Acetylation of the protein N-terminus, pyroglutamate formation of N-terminal glutamine, methionine oxidation to methionine-sulfoxide, and phosphorylation of serine, threonine, and tyrosine were set as variable modifications. The protease setting was set to trypsin with one missed cleavage allowed. The mass tolerance on precursor ions was set to ±10 ppm and on fragment ions to ±0.5 Da. In addition, Mascot's C13 setting was set to 1. Only peptides that were ranked 1 and had an ion score at least equal to the corresponding identity threshold at 99% confidence were withheld, and further data handling was done in the ms_lims database (Helsens *et al.*, 2010).

Phosphatase assay

We preincubated 0.2 µM GST-XSSH or GST-XSSH phosphorylated with CSF extracts (pXSSH) with or without 4.7 µM F-actin for 15 min at 22°C and then added 10 µM pXAC to the mixture to start monitoring the phosphatase activity. A 4-µl amount of the mixture was removed and mixed with the same volume of SDS-sample buffer to stop the reaction and was applied to SDS–PAGE.

Pull-down assay

We absorbed 20 µg of GST-tail, GST–N-tail, or GST–C-tail with or without phosphorylation with CSF extracts to 20 µl of glutathione-beads and incubated with 40 µl of 3.3 µM 14-3-3ζ in F-buffer containing 1% bovine serum albumin with gentle stirring at 22°C for 1 h. The beads were washed with F-buffer containing 0.1% Triton X-100 and applied to SDS–PAGE.

Sedimentation assay

Binding of XSSH and XAC to actin filaments was examined by the sedimentation assay. Actin (4.7 µM) and various concentrations of XSSH in the absence or presence of chick cofilin (4.7 µM) were mixed and incubated at 22°C for 3 h. Buffer composition was 60 mM KCl, 2 mM $MgCl_2$, 1 mM DTT, and 20 mM HEPES-KOH, pH 7.2. Mixtures were then ultracentrifuged at 436,000 × *g* for 20 min, and the supernatant and pellet were subjected to SDS–PAGE.

Immunodepletion

Immunodepletion of XSSH from CSF extracts was performed by using anti-XSSH rabbit polyclonal antibody according to Rosenblatt *et al.* (1997). Mock-depleted CSF extracts were prepared by incubating CSF extracts at 4°C for 1 h with protein G–Sepharose beads (GE Healthcare) preequilibrated with CSF-XB. The pellet was removed by centrifugation at 12,000 × g for 20 s.

Microinjection into oocytes

Purified anti-XSSH IgG was dialyzed against 60 mM KCl, 2 mM $MgCl_2$, and 5 mM HEPES-KOH, pH 7.2. Injection volumes from a pressure injector (CIJ-1; Shimadzu, Kyoto, Japan) were calibrated by measuring the volume of an aqueous drop delivered into mineral oil. Injections were given in OR2 medium containing 5% Ficoll PM400 (GE Healthcare) by inserting a glass needle into the marginal zone of an oocyte in a volume of 30 nl per oocyte. After injection, the injected oocytes were incubated in OR2 medium for 2 h at 16°C and then treated with progesterone to induce oocyte maturation at 19°C.

Immunofluorescence microscopy

Oocytes were fixed in OR2 medium containing 3.7% formaldehyde and 1% trichloroacetic acid for 2 h at room temperature with gentle tumbling in a rotation mixer and then transferred to 70% ethanol (3 × 30 min) and stored at −20°C. Oocytes were dehydrated sequentially with 90, 95%, 99.5, and 100% ethanol, cleared with toluene, and embedded in paraffin. Sections (8 µm thick) were cut out and mounted on MAS-coat slide glass (Matsunami Glass, Osaka, Japan). Paraffin was removed with xylol, and the specimens were rehydrated sequentially with ethanol and finally with PBS. For antigen retrieval, the specimens were heated in a Tris-EDTA buffer (1 mM EDTA, 0.05% Tween 20, 10 mM Tris-HCl, pH 9.0) for 20 min at 100°C and then placed in cold water for 10 min. After blocking with 20% goat serum in PBS for >1 h, the sections were incubated with anti-actin antibody or anti-tubulin (DM1A) antibodies for 1 h at room temperature and then with fluorescein isothiocyanate–labeled secondary antibody. After each immunoreaction step, the sections were rinsed and washed with PBS. The sections were mounted in PBS containing 1 mg/ml *p*-phenylenediamine and 90% glycerol.

ACKNOWLEDGMENTS

We are grateful to Kazuko Iida for anti-actin antibody, Takeo Kishimoto for pGEX-ΔN85 cyclin B2 vector, and James R. Bamburg for anti–phospho-ADF/cofilin antibody. S.O. was supported by National Institutes of Health Grant R01 AR48615.

REFERENCES

Abe H, Obinata T, Minamide LS, Bamburg JR (1996). *Xenopus laevis* actin-depolymerizing factor/cofilin: a phosphorylation-regulated protein essential for development. J Cell Biol 132, 871–885.

Arber S, Barbayannis FA, Hanser H, Schneider C, Stanyon CA, Bernard O, Caroni P (1998). Regulation of actin dynamics through phosphorylation of cofilin by LIM-kinase. Nature 393, 805–809.

Azoury J, Lee KW, Georget V, Hikal P, Verlhac MH (2011). Symmetry breaking in mouse oocytes requires transient F-actin meshwork destabilization. Development 138, 2903–2908.

Azoury J, Lee KW, Georget V, Rassinier P, Leader B, Verlhac MH (2008). Spindle positioning in mouse oocytes relies on a dynamic meshwork of actin filaments. Curr Biol 18, 1514–1519.

Barišič S, Nagel AC, Franz-Wachtel M, Macek B, Preiss A, Link G, Maier D, Hausser A (2011). Phosphorylation of Ser 402 impedes phosphatase activity of slingshot 1. EMBO Rep 12, 527–533.

Becker BE, Romney SJ, Gard DL (2003). XMAP215, XKCM1, NuMA, and cytoplasmic dynein are required for the assembly and organization of the transient microtubule array during the maturation of *Xenopus* oocytes. Dev Biol 261, 488–505.

Bernstein BW, Bamburg JR (2010). ADF/cofilin: a functional node in cell biology. Trends Cell Biol 20, 187–195.

Bohnsack MT, Stüven T, Kuhn C, Cordes VC, Görlich DA (2006). Selective block of nuclear actin export stabilizes the giant nuclei of *Xenopus* oocytes. Nat Cell Biol 8, 257–263.

Calarco PG (2005). The role of microfilaments in early meiotic maturation of mouse oocytes. Microsc Microanal 11, 146–153.

Dahlgaard K, Raposo AASF, Niccoli T, St Johnston D (2007). Capu and Spire assemble a cytoplasmic actin mesh that maintains microtubule organization in the *Drosophila* oocyte. Dev Cell 13, 539–553.

Deng M, Li R (2009). Sperm chromatin-induced ectopic polar body extrusion in mouse eggs after ICSI and delayed egg activation. PLoS One 4, e7171.

Deng M, Suraneni P, Schultz RM, Li R (2007). The Ran GTPase mediates chromatin signaling to control cortical polarity during polar body extrusion in mouse oocytes. Dev Cell 12, 301–8.

Dorée M, Hunt T (2002). From Cdc2 to Cdk1: when did the cell cycle kinase join its cyclin partner? J Cell Sci 115, 2461–2464.

Eiseler T, Döppler H, Yan IK, Kitatani K, Mizuno K, Storz P (2009). Protein kinase D1 regulates cofilin-mediated F-actin reorganization and cell motility through slingshot. Nat Cell Biol 11, 545–556.

Field CM, Lénárt P (2011). Bulk cytoplasmic actin and its functions in meiosis and mitosis. Curr Biol 21, 825–830.

Gard DL (1992). Microtubule organization during maturation of *Xenopus* oocytes: assembly and rotation of the meiotic spindles. Dev Biol 151, 516–530.

Gard DL, Cha BJ, Roeder AD (1995). F-actin is required for spindle anchoring and rotation in *Xenopus* oocytes: a re-examination of the effects of cytochalasin B on oocyte maturation. Zygote 3, 17–26.
Ghesquière B *et al.* (2009). In vitro and in vivo protein-bound tyrosine nitration characterized by diagonal chromatography. Mol Cell Proteomics 8, 2642–2652.
Glotzer M, Murray A, Kirschner MW (1991). Cyclin is degraded by the ubiquitin pathway. Nature 349, 132–138.
Helsens K *et al.* (2010). ms_lims, a simple yet powerful open source laboratory information management system for MS-driven proteomics. Proteomics 10, 2560.
Iida K, Yahara I (1986). Reversible induction of actin rods in mouse C3H-2K cells by incubation in salt buffers and by treatment with non-ionic detergents. Exp Cell Res 164, 492–506.
Jessus C, Huchon D, Ozon R (1986). Distribution of microtubules during the breakdown of the nuclear envelope of the *Xenopus* oocyte: an immunocytochemical study. Biol Cell 56, 113–120.
Kligys K, Claiborne JN, DeBiase PI, Hopkinson SB, Wu Y, Mizuno K, Jones JC (2007). The slingshot family of phosphatases mediates Rac1 regulation of cofilin phosphorylation, laminin-332 organization, and motility behavior of keratinocytes. J Biol Chem 282, 32520–32528.
Laemmli UK (1970). Cleavage of structural proteins during the assembly of the head of bacteriophage T4. Nature 227, 680–685.
Lénárt P, Bacher CP, Daigle N, Hand AR, Eils R, Terasaki M, Ellenberg J (2005). Contractile nuclear actin network drives chromosome congression in oocytes. Nature 436, 812–818.
Liu JL, Sung LY, Tian XC, Yang X (2002). Hypertonicity-induced projections reflect cell polarity in mouse metaphase II oocytes: involvement of microtubules, microfilaments, and chromosomes. Biol Reprod 67, 1853–1863.
Lohka MJ, Hayes MK, Maller JL (1988). Purification of maturation-promoting factor, an intracellular regulator of early mitotic events. Proc Natl Acad Sci USA 85, 3009–3013.
Longo FJ, Chen DY (1985). Development of cortical polarity in mouse eggs: involvement of the meiotic apparatus. Dev Biol 107, 382–394.
Margalit A, Vlcek S, Gruenbaum Y, Foisner R (2005). Breaking and making of the nuclear envelope. J Cell Biochem 95, 454–465.
Masui Y, Clarke HJ (1979). Oocyte maturation. Int Rev Cytol 57, 185–282.
Masui Y, Markert CL (1971). Cytoplasmic control of nuclear behavior during meiotic maturation of frog oocytes. J Exp Zool 177, 129–145.
Meberg PJ, Ono S, Minamide LS, Takahashi M, Bamburg JR (1998). Actin depolymerizing factor and cofilin phosphorylation dynamics: response to signals that regulate neurite extension. Cell Motil Cytoskeleton 39, 172–190.
Miyamoto K, Pasque V, Jullien J, Gurdon JB (2011). Nuclear actin polymerization is required for transcriptional reprogramming of Oct4 by oocytes. Genes Dev 25, 946–958.
Mori M, Monnier N, Daigle N, Bathe M, Ellenberg J, Lénárt P (2011). Intracellular transport by an anchored homogeneously contracting F-actin meshwork. Curr Biol 21, 606–611.
Murray AW (1991). Cell cycle extracts. Methods Cell Biol 36, 581–605.
Nagaoka R, Abe H, Obinata T (1996). Site-directed mutagenesis of the phosphorylation site of cofilin: its role in cofilin-actin interaction and cytoplasmic localization. Cell Motil Cytoskeleton 35, 200–209.
Nagaoka R, Kusano K, Abe H, Obinata T (1995). Effects of cofilin on actin filamentous structures in cultured muscle cells: intracellular regulation of cofilin action. J Cell Sci 108, 581–593.
Nagata-Ohashi K *et al.* (2004). A pathway of neuregulin-induced activation of cofilin-phosphatase Slingshot and cofilin in lamellipodia. J Cell Biol 165, 465–471.
Niwa R, Nagata-Ohashi K, Takeichi M, Mizuno K, Uemura T (2002). Control of actin reorganization by Slingshot, a family of phosphatases that dephosphorylate ADF/cofilin. Cell 108, 233–246.
O'Farrell PG, Goodman HM, O'Farrell PH (1977). High resolution two-dimensional electrophoresis of basic as well as acidic proteins. Cell 12, 1133–1141.
Okada I, Fujiki S, Iwase S, Abe H (2012). Stabilization of actin filaments prevents germinal vesicle breakdown and affects microtubule organization in *Xenopus* oocytes. Cytoskeleton 69, 312–323.
Okada K, Obinata T, Abe H (1999). XAIP1: a *Xenopus* homologue of yeast actin interacting protein 1 (AIP1), which induces disassembly of actin filaments cooperatively with ADF/cofilin family proteins. J Cell Sci 112, 1553–1565.
Ono S (2007). Mechanism of depolymerization and severing of actin filaments and its significance in cytoskeletal dynamics. Int Rev Cytol 258, 1–82.
Pfender S, Kuznetsov V, Pleiser S, Kerkhoff E, Schuh M (2011). Spire-type actin nucleators cooperate with Formin-2 to drive asymmetric oocyte division. Curr Biol 21, 955–960.
Pollard TD, Cooper JA (2009). Actin, a central player in cell shape and movement. Science 326, 1208–1212.
Prodon F, Hanawa K, Nishida H (2009). Actin microfilaments guide the polarized transport of nuclear pore complexes and the cytoplasmic dispersal of Vasa mRNA during GVBD in the ascidian *Halocynthia roretzi*. Dev Biol 330, 377–388.
Prodon F, Sardet C, Nishida H (2008). Cortical and cytoplasmic flows driven by actin microfilaments polarize the cortical ER-mRNA domain along the a-v axis in ascidian oocytes. Dev Biol 313, 682–699.
Rosenblatt J, Agnew BJ, Abe H, Bamburg JR, Mitchison TJ (1997). *Xenopus* actin depolymerizing factor/cofilin (XAC) is responsible for the turnover of actin filaments in *Listeria monocytogenes* tail. J Cell Biol 136, 1323–1332.
Ryabova LV, Betina MI, Vassetzky SG (1986). Influence of cytochalasin B on oocyte maturation in *Xenopus laevis*. Cell Differ 19, 89–96.
Sandquist JC, Kita AM, Bement WM (2011). And the dead shall rise: actin and myosin return to the spindle. Dev Cell 21, 410–419.
Schuh M, Ellenberg J (2008). A new model for asymmetric spindle positioning in mouse oocytes. Curr Biol 18, 1986–1992.
Soosairajah J, Maiti S, Wiggan O, Sarmiere P, Moussi N, Sarcevic B, Sampath R, Bamburg JR, Bernard O (2005). Interplay between components of a novel LIM kinase-slingshot phosphatase complex regulates cofilin. EMBO J 24, 473–486.
Spudich JA, Watt S (1971). The regulation of rabbit skeletal muscle contraction. I. Biochemical studies of the interaction of the tropomyosin-troponin complex with actin and the proteolytic fragments of myosin. J Biol Chem 246, 4866–4871.
Sun QY, Schatten H (2006). Regulation of dynamic events by microfilaments during oocyte maturation and fertilization. Reproduction 131, 193–205.
Takahashi T, Koshimizu U, Abe H, Obinata T, Nakamura T (2001). Functional involvement of *Xenopus* LIM kinases in progression of oocyte maturation. Dev Biol 229, 554–567.
Tanaka K, Nishio R, Haneda K, Abe H (2005a). Functional involvement of *Xenopus* homologue of ADF/cofilin phosphatase, Slingshot (XSSH), in the gastrulation movement. Zool Sci 22, 955–969.
Tanaka K, Okubo Y, Abe H (2005b). Involvement of slingshot in the Rho-mediated dephosphorylation of ADF/cofilin during *Xenopus* cleavage. Zool Sci 22, 971–984.
Towbin H, Staehelin T, Gordon J (1979). Electrophoretic transfer of proteins from polyacrylamide gels to nitrocellulose sheets: procedure and some applications. Proc Natl Acad Sci USA 76, 4350–4354.
Van Troys MV, Huyck L, Leyman S, Dhaese S, Vandekerkhove J, Ampe C (2008). Ins and outs of ADF/cofilin activity and regulation. Eur J Cell Biol 87, 649–667.
Verlhac MH (2011). Spindle positioning: going against the actin flow. Nat Cell Biol 13, 1183–1185.
Verlhac MH, Lefebvre C, Guillaud P, Rassinier P, Maro B (2000). Asymmetric division in mouse oocytes: with or without Mos. Curr Biol 10, 1303–1306.
Weber KL, Sokac AM, Berg JS, Cheney RE, Bement WM (2004). A microtubule-binding myosin required for nuclear anchoring and spindle assembly. Nature 431, 325–329.
Wessel D, Flugge UI (1984). A method for the quantitative recovery of protein in dilute solution in the presence of detergents and lipids. Anal Biochem 138, 141–143.
Yang N, Higuchi O, Ohashi K, Nagata K, Wada A, Kangawa K, Nishida E, Mizuno K (1998). Cofilin phosphorylation by LIM-kinase 1 and its role in Rac-mediated actin reorganization. Nature 393, 809–812.
Yi K, Unruh JR, Deng M, Slaughter BD, Rubinstein B, Li R (2011). Dynamic maintenance of asymmetric meiotic spindle position through Arp2/3-complex-driven cytoplasmic streaming in mouse oocytes. Nat Cell Biol 13, 1252–1258.